Materials Advances

ROYAL SOCIETY OF CHEMISTRY

PAPER

View Article Online
View Journal | View Issue

Cite this: *Mater. Adv.*, 2024, 5, 5134

A triphenylamine functionalized photosensitizer as a promising candidate for osteosarcoma cancer phototheranostics†

Chongchong Yin,[a] Xiaowen Bao,[b] Jiaqi Li,[b] Jianwei Zhu[b] and Jisheng Sui *[a]

Received 11th October 2023,
Accepted 1st May 2024

DOI: 10.1039/d3ma00835e

rsc.li/materials-advances

Osteosarcoma is a malignant tumor affecting an increasing number of individuals worldwide. In this paper, a triphenylamine (TPA) functionalized photosensitizer DPPTPA was synthesized for cancer theranostics. The conjugation of TPA onto the DPP moiety not only prolongs the absorbance to the near-infrared region (NIR) but also adds to the phototoxicity of DPPTPA. DPPTPA NPs prepared by the nanoprecipitation method exhibit considerable cytotoxicity under laser irradiation, with a half-maximal inhibitory concentration (IC_{50}) of 4.38 μg mL^{-1} for inhibiting HOS cell proliferation. The green channel of a confocal laser scanning microscope confirmed efficient cellular uptake. Furthermore, *in vivo* studies indicated that tumor proliferation was suppressed effectively upon laser irradiation. In contrast, the tumor volume in the non-irradiation group remained like that in the control group, indicating high phototoxicity and low dark toxicity. The results demonstrate the potential of DPPTPA nanoparticles for cancer phototheranostics.

1 Introduction

In the past few decades, significant efforts have been made towards phototherapy, owing to its advantages over traditional therapies, such as non-invasiveness, diminished side effects, and excellent biocompatibility.[1–5] Ideal phototherapy induces cell apoptosis, leading to tumor regression through the photogeneration of reactive oxygen species (ROS) or heat.[6–13] Photosensitizers (PSs), the fundamental component of phototherapy, are crucial for therapeutic efficacy. Therefore, designing and synthesizing appropriate PSs are the key to enhancing the ROS generation ability and photothermal conversion efficiency.[14–17]

Among the various photosensitizers, semiconducting compounds are organic electronic materials with π conjugated polymer backbones consisting of double bonds or aromatic rings.[18–22] Their overlapping p-orbitals lead to the formation of highly delocalized electrons, thereby enabling them to show outstanding optoelectronic properties.[23–30] For example, Shen *et al.* reported a semiconducting polymer for photodynamic and photothermal therapy.[11] Another example is that Zou *et al.* used 2-pyridione functionalized PEG to capture and release singlet oxygen generated from the photosensitization of a semiconducting compound DPPTPE for cancer theranostics.[31] In this paper, a triphenylamine (TPA) functionalized DPP compound with efficient intersystem crossing for PDT is reported (Scheme 1). The conjugation of TPA not only enhances the ROS generation ability of DPPTPA but also prolongs the absorbance to the NIR. The as-obtained DPPTPA NPs by nanoprecipitation possess high ROS generation ability and show a low half-maximal inhibitory concentration of 4.38 μg mL^{-1} for human osteosarcoma HOS cell lines. Furthermore, *in vivo* studies indicate that such NPs can induce tumor regression efficiently with the help of laser and exert no apparent lesions and injuries on major organs (including the heart, liver, spleen, lungs, and kidneys). The results indicate that DPPTPA NPs are potential candidates for osteosarcoma cancer phototheranostics.

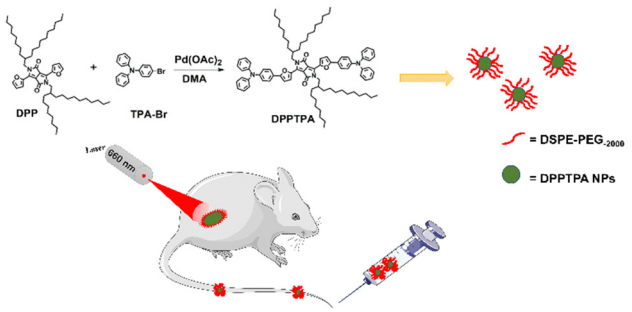

Scheme 1 Illustration of DPPTPA NPs for PDT therapy.

[a] Department of Orthopaedic Surgery, Nanjing First Hospital, Nanjing Medical University, 210000, Nanjing, Jiangsu, China. E-mail: suijisheng@njmu.edu.cn
[b] School of Pharmaceutical Sciences, Nanjing Tech University (NanjingTech), 30 South Puzhu Road, Nanjing 211816, China

† Electronic supplementary information (ESI) available. See DOI: https://doi.org/10.1039/d3ma00835e

2 Experimental section

2.1 Materials

The human osteosarcoma cell lines HOS were obtained from the Cell Bank of the Shanghai Institute of Biochemistry and Cell Biology, Chinese Academy of Sciences. Minimum essential medium (MEM) and fetal bovine serum (FBS) were provided by Gibco Life Technologies (New York, USA). Antibiotics 100× (penicillin: 100 IU mL^{-1}, streptomycin 100 μg mL^{-1}) were purchased from Thermo Fisher Scientific (USA). Five-week-old male BALB/c nude mice were obtained from the Comparative Medicine Center, at Yangzhou University. The handling of animals in all the animal studies was carried out with ethical approval and performed according to the Experimental Animals Administrative Committee of Nanjing Medical University.

2.2 Synthesis of DPPTPA and NPs

A mixture of DPP (200.0 mg, 0.24 mmol), 4-bromotriphenylamine (194.4 mg, 0.60 mmol), platinum acetate (11.0 mg, 0.02 mmol), pivalic acid (20 mg, 0.20 mmol) and K_2CO_3 (83.0 mg, 0.60 mmol) was dissolved in 5 mL of *N*,*N*-dimethyl acetamide (DMA). Then, N_2 was bubbled to drive off possible oxygen and water in the system. Under the protection of N_2, the mixture was heated to 110 °C for 12 h. The mixture was poured into a saturated sodium chloride solution (150 mL) and extracted with 100 mL dichloromethane three times after cooling to room temperature. The solvent was removed using rotary evaporation and purified using silica gel column chromatography with dichloromethane and hexane (1 : 2, v/v) as the developing solvent. Dark blue solids were obtained (yield: 30%). ^{1}H NMR: δ H 7.63–7.40 (2H, d), 7.28–7.20 (10H, m), 7.11–7.04 (10H, m), 7.03–6.96 (10H, m), 4.15–4.00 (4H, d), 1.89 (2H, s), 1.26–1.06 (63H, m), and 0.81–0.74 (13H, m). The nanoparticles (NPs) of DPPTPA were prepared by nanoprecipitation with DSPE-PEG. A mixture of DSPE-PEG (10 mg) and DPPTPA (5 mg) was dissolved in tetrahydrofuran (THF, 1 mL). Then, 200 mL of this solution was dropped into distilled water (10 mL) with ultrasound treatment at room temperature. The mixture was stirred overnight to remove THF.

2.3 Cell culture and MTT assay

HOS cells were cultured in MEM culture medium supplemented with 10% fetal bovine serum and 1% antibiotics (penicillin: 100 IU mL^{-1}, streptomycin: 100 μg mL^{-1}). The cells were cultured in a humidified incubator with 5% CO_2 at 37 °C. *In vitro* cell viability was assessed using a 3-(4,5-dimethylthiazol-2-yl)-2,5-diphenyltetrazolium bromide (MTT) colorimetric assay. Cells were seeded at a density of 1×10^4 cells per well in 100 μl of culture medium in 96-well plates and incubated for 24 hours. The DPPTPA NPs were diluted with MEM to various concentrations, added into the 96-well plate, and incubated for another 12 h, while the control cells were treated with 0.5% DMSO. The 96-well plate was irradiated for 10 minutes with a laser at 660 nm and 0.2 W cm^{-2} or 1 W cm^{-2}. After that, the cells were still incubated for another 12 h; after irradiation, 10 μL of the MTT solution (5 mg mL^{-1} in PBS) was added and incubated for 4 hours. Supernatants were removed, and 100 μL of DMSO per well was added at approximately 25 °C to dissolve formazan crystals. The absorbance was measured at 492 nm using a Thermo Multiskan Mk3 Microplate Reader. Cell growth inhibitory effects were calculated using the following formula: cell viability (%) = ($A_{treatment}$/$A_{control}$) × 100%. The half-maximal inhibitory concentration (IC_{50}) was determined using GraphPad Prism 6 software (GraphPad Software, Inc., La Jolla, CA, USA).

2.4 Cellular uptake study

Cellular uptake of DPPTPA NPs by HOS cells was evaluated using fluorescence inverted microscopy and flow cytometry. HOS cells were incubated with 2 mL of DPPTPA NPs at a concentration of 1 μg mL^{-1} in a confocal dish for 24 hours in a 5% CO_2 incubator. After incubation, the cells were washed thrice with cold PBS and fixed with 4% paraformaldehyde for 15 minutes. Fluorescence images were observed using an Olympus IX70 inverted microscope, excited at 633 nm laser, and collected from 650 to 750 nm.

2.5 Annexin V-FITC/propidium iodide (PI) staining

Apoptosis was analysed using annexin V-FITC/propidium iodide (PI) dual staining. HOS cells were seeded into a 6-well culture plate and divided into three groups: control, illumination, and without illumination groups. Then, cells were harvested after treatment with DPPTPA NPs (10 μg mL^{-1}, 2 mL) for 24 h, stained using the Annexin V-FITC/PI cell apoptosis detection kit (KeyGen Biotech, Nanjing, China). The apoptosis rates of the cells were then analyzed using a flow cytometer (BD Biosciences, San Jose, CA, USA).

2.6 Antitumor effects on nude mice

To conduct a tumor suppression study, we established xenograft tumor models using female BALB/c nude mice aged 35–40 days (20 ± 2 g), which were obtained from the Comparative Medicine Centre of Yangzhou University. The animal study was conducted in accordance with the regulations of the National Institutes of Health and approved by the Institutional Animal Care and Use Committee (IACUC) of Nanjing Medical University. The mice were kept in a controlled environment at a temperature of 21 ± 2 °C, a humidity of 45 ± 10%, and a 24-hour light/dark cycle throughout the study. The HOS cells, at a density of 5×10^6 cells per 100 μL serum-free medium, were subcutaneously injected into the right flank of each nude mouse. The tumor size was measured every two days, and when the tumor volume reached approximately 100 mm^3, the mice were randomly divided into four groups: (1) control group; (2) DPPTPA NP (laser−) group; (3) DPPTPA NP (0.2 W cm^{-2}) group; and (4) DPPTPA NP (1 W cm^{-2}) group. The control group was administered with saline, while the other three groups were administered with DPPTPA NPs (100 μg mL^{-1}, 100 μL). After administration, the tumors of the control and illumination groups were irradiated with 660 nm laser (0.2 W cm^{-2}) for 10 minutes, while the mice in the group without illumination were not irradiated. The tumor volume was calculated using the formula: $V = 1/2 \times L \times W^2$, where "*L*" and "*W*" represent the longest and shortest diameters of the tumors, respectively.

After the 14-day treatment process, the tumor volume and body weight of the mice were measured every other day. At the end of the study, the mice were euthanized with CO_2, and their tumor tissues and major organs were collected for histopathological analysis.

2.7 Statistical analysis

All the data were expressed as mean values ± standard deviations (mean ± SD). One-way analysis of variance (ANOVA) was used to compare among the treatment groups. $P \leq 0.05$ was considered statistically significant.

3 Results and discussion

3.1 Synthesis of DPPTPA, NPs and ROS generation ability

DPPTPA was synthesized by the conjugation of triphenylamine onto DPP and characterized by ^{1}H NMR (Fig. S1, ESI†). The nanoprecipitation method was used to synthesize water-dispersible nanoparticles (NPs) for biological applications. To investigate the responsiveness of DPPTPA to NIR light, the absorbance of DPPTPA and NPs was recorded (Fig. 1A). A blue shift of DPPTPA NPs in water was observed, compared with that in THF, which is attributed to the aggregation of DPPTPA in water. A similar phenomenon was observed in the emission spectra (Fig. 1B). Dynamic light scattering (DLS) results show that such NPs have a uniform size distribution with an average size of 65 nm (Fig. 1C), and these results are consistent with those of TEM (Fig. 1D). The small size will contribute to the cellular uptake of the NPs *in vivo*. For an excellent photosensitizer, strong ROS generation ability guarantees superior phototherapeutic efficacy. To investigate the generation of ROS by DPPTPA in dichloromethane, the absorbance of DPBF was recorded while irradiated (Fig. 1E and F). The continuous absorbance degradation indicates the efficient ROS generation ability.

3.2 Cellular uptake, MTT assay and flow cytometry in human osteosarcoma cells

The cellular uptake process of DPPTPA NPs in HOS cells was confirmed using a confocal imaging system (Fig. 2A). A high intracellular fluorescence intensity was observed in the cytoplasmic matrix, indicating that the DPPTPA NPs can be used for cell imaging *in vitro*. In addition, 2′,7′-dichlorofluorescein diacetate (DCF-DA) was used to investigate the singlet oxygen detection generation efficacy of DPPTPA NPs in HOS cells. As shown in Fig. 2A, DPPTPA NPs can produce potent singlet oxygen with light irradiation, which is evident from the intense green fluorescence observed. This highlights the potential of DPPTPA NPs for ROS generation.

To confirm the therapeutic potential of DPPTPA NPs, we assessed their ability to inhibit the viability of HOS human osteosarcoma cells at various concentrations. After treatment of DPPTPA NPs for 24 h, the MTT assay shows that the IC_{50} (the concentration of drug inhibiting 50% of cells) value was 4.38 μg mL^{-1} (Fig. 2B). Moreover, the group treated with nanoparticles in the absence of light exhibited minimal dark toxicity. These data demonstrated that DPPTPA NPs had an excellent inhibitory effect on osteosarcoma cells and low dark toxicity. The cytotoxicity of DPPTPA NPs is higher than that of the previously reported PDPP (13.84 μg mL^{-1}).[36] The pro-apoptotic effect of DPPTPA NPs was confirmed by using the Annexin V-FITC/PI double staining assay (Fig. 2C). The apoptotic rates of HOS cells were significantly increased in the illumination group after treatment with DPPTPA NPs (5 μg mL^{-1}), as demonstrated by annexin V-FITC/PI double staining assay. In contrast, the apoptotic rate of the group treated with DPPTPA NPs without illumination was similar to that of the control group (Fig. 2C), which indicated that DPPTPA NPs could induce typical apoptosis in human osteosarcoma cells under irradiation.

3.3 *In vivo* phototherapy

In this study, nude mice with osteosarcoma tumors were used to investigate further the *in vivo* photodynamic therapy (PDT) anti-tumor efficacy of DPPTPA NPs. As shown in Fig. 3A, the relative tumor volume of the control and without illumination groups increases nearly 13-fold. In contrast, the relative tumor volume of the DPPTPA NP (0.2 W cm^{-2}) group increased by 1.7-fold. In comparison, tumors in the DPPTPA NP (1 W cm^{-2})

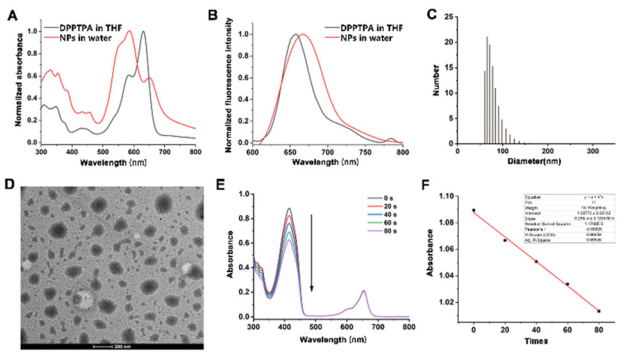

Fig. 1 (A) Normalized absorbance of DPPTPA in THF and NPs in water. (B) Normalized fluorescence spectra of DPPTPA in THF and NPs in water. (C) Dynamic light scattering of DPPTPA NPs. (D) TEM of NPs. (E) Degradation of the absorbance of DPBF in the presence of DPPTPA in dichloromethane with laser irradiation. (F) Linear fitting of the time *versus* absorbance.

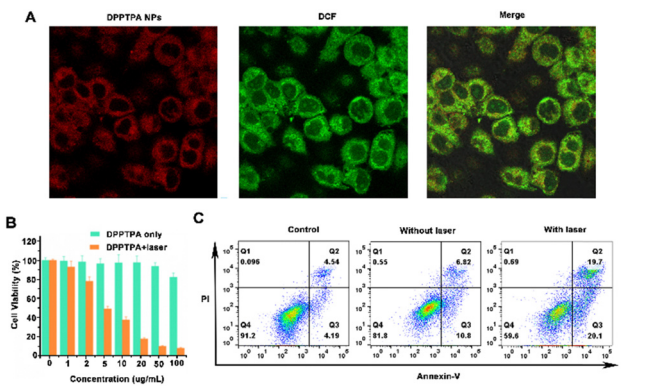

Fig. 2 (A) Cellular uptake of DPPTPA NPs in HOS cells. (B) MTT assay of DPPTPA NPs in HOS cells with/without irradiation. (C) Flow cytometry of DPPTPA NPs in HOS cells indicates cell apoptosis with irradiation.

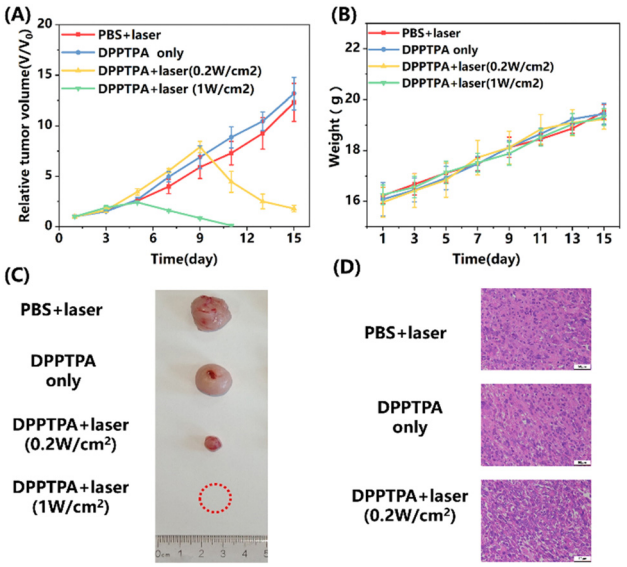

Fig. 3 (A) Tumor volume change of the mice. (B) Body weight change. (C) Representative tumor pictures. (D) H&E stained photos of the tumors in the PBS + laser, DPPTPA only, and DPPTPA + laser (0.2 W cm^{-2}) groups.

group gradually shrunk and completely disappeared after being treated 6 times at the end of the therapy process. Compared with the control group, DPPTPA NPs can inhibit tumor growth and even eliminate tumor cells completely after laser irradiation. These results suggest that DPPTPA NPs exhibit excellent phototoxicity and efficiency in treating tumors. In addition, the potential toxicity of DPPTPA NPs must be assessed by monitoring the weight changes of nude mice. During the treatment process, we found that each group has no significant difference in the weights of nude mice (Fig. 3B), suggesting the low dark toxicity of DPPTPA NPs. Representative tumor pictures in the four groups are illustrated in Fig. 4c. Additionally, H&E staining of tumor tissues indicated that the control and DPPTPA (laser−) groups had a higher number of tumor cells with larger nuclei compared to the other treatment groups. In contrast, DPPTPA NPs with laser groups have notable necrosis. These results demonstrate that DPPTPA NPs exerted strong anti-tumor activity (Fig. 3D).

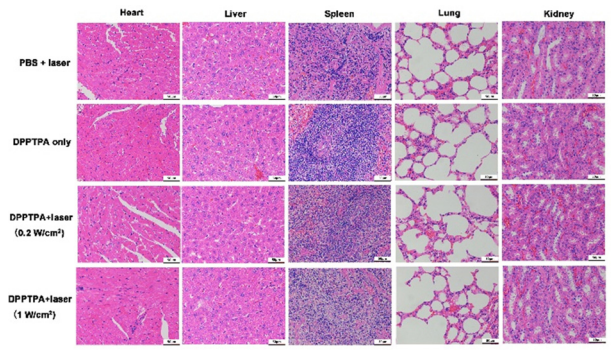

Fig. 4 H&E pictures of the heart, liver, spleen, lungs, and kidneys. Scale bar: 10 μm.

All mice were euthanized to investigate the possible damage to the tumor and other tissues after treatment, and their organs, including heart, liver, spleen, lungs, and kidneys, were collected for further analysis. The results from the H&E staining pictures are shown in Fig. 4. No apparent tissue damage was found in comparison with the control group according to H&E staining of major organs, and minimal toxicity *in vivo*, and have a great prospect in clinical use.[32–35] Furthermore, the TUNEL results indicate that positive cells in tumor tissues with DPPTPA (laser+) increased significantly, compared with those of the control group (Fig. S2, ESI†).

4 Conclusion

In conclusion, we have reported a triphenylamine functionalized DPPTPA for treating osteosarcoma. DPPTPA with NIR absorbance can generate singlet oxygen efficiently when responding to a laser. DPPTPA NPs can be endocytosed by HOS cells, and the half-maximal inhibitory concentration is as low as 4.38 μg mL^{-1} with laser irradiation, which is consistent with the flow cytometry results. Further *in vivo* investigation demonstrates that DPPTPA NPs can suppress tumor proliferation with the help of a laser, leading to tumor regression completely under high laser power. The results will provide some evidence for DPPTPA NPs for pre-clinical trials.

Author contributions

Chongchong Yin is mainly responsible for synthesizing and characterizing compounds, Xiaowen Bao is primarily responsible for cell experiments and writing, and Jiaqi Li is responsible for animal experiments and drug administration *in vivo*. Jianwei Zhu is responsible for animal experiments and tissue sample staining, and Jisheng Sui is mainly accountable for experimental design and guidance.

Conflicts of interest

The authors have no conflict of interest to declare.

Acknowledgements

The authors acknowledge the financial support from the National Natural Science Foundation of China (No. 81771985) and the Nanjing Science and Technology Plan Project (202308004).

References

1 H. Chen, W. Zhang, G. Zhu, X. Jin and X. Chen, Rethinking cancer, *Nat. Rev. Mater.*, 2017, **2**(7), 17024.
2 I. Mura and P. Couvreur, Nanotheranostics for personalized medicine, *Adv. Drug Delivery Rev.*, 2012, **64**(13), 1394–1416.
3 M. S. Muthu, D. T. Leong, L. Mei and S. S. Feng, Nanotheranostics - application and further development of nanomedicine

strategies for advanced theranostics, *Theranostics*, 2014, **4**(6), 660–677.
4 E. K. Lim, T. Kim, S. Paik, S. Haam, Y. M. Huh and K. Lee, Nanomaterials for theranostics: recent advances and future challenges, *Chem. Rev.*, 2015, **115**(1), 327–394.
5 X. Chen, G. Zheng, J. Cheng and Y. Y. Yang, Supramolecular Nanotheranostics, *Theranostics*, 2019, **9**(11), 3014–3016.
6 Y. Liu, P. Bhattarai, Z. Dai and X. Chen, Photothermal therapy and photoacoustic imaging via nanotheranostics in fighting cancer, *Chem. Soc. Rev.*, 2019, **48**(7), 2053–2108.
7 D. Ni, C. A. Ferreira, T. E. Barnhart, V. Quach, B. Yu, D. Jiang, W. Wei, H. Liu, J. W. Engle, P. Hu and W. Cai, Magnetic Targeting of Nanotheranostics Enhances Cerenkov Radiation-Induced Photodynamic Therapy, *J. Am. Chem. Soc.*, 2018, **140**(44), 14971–14979.
8 J. Zou, Z. Yin, P. Wang, D. Chen, J. Shao, Q. Zhang, L. Sun, W. Huang and X. Dong, Photosensitizer synergistic effects: D–A–D structured organic molecule with enhanced fluorescence and singlet oxygen quantum yield for photodynamic therapy, *Chem. Sci.*, 2018, **9**(8), 2188–2194.
9 J. Zhu, J. Zou, J. Zhang, Y. Sun, X. Dong and Q. Zhang, Anthracene functionalized bodipy derivative with singlet oxygen storage ability for photothermal and continuous photodynamic synergistic therapy, *J Mater. Chem. B*, 2019, **7**, 3303–3309.
10 L. Feng, C. Zhu, H. Yuan, L. Liu, F. Lv and S. Wang, Conjugated polymer nanoparticles: preparation, properties, functionalization and biological applications, *Chem. Soc. Rev.*, 2013, **42**(16), 6620–6633.
11 J. Shen, J. Chen, Z. Ke, D. Zou, L. Sun and J. Zou, Heavy atom-free semiconducting polymer with high singlet oxygen quantum yield for prostate cancer synergistic phototherapy, *Mater. Chem. Front.*, 2019, **3**(6), 1123–1127.
12 J. Deng, N. Zhong, X. Zhang, C. Li, C. Xu and J. Zhao, A carbazole functionalized semiconducting compound as a heavy atom free photosensitizer for phototherapy against lung cancer, *J. Mater. Chem. B*, 2020, **8**(47), 10764–10769.
13 W. Tang, Z. Yang, S. Wang, Z. Wang, J. Song, G. Yu, W. Fan, Y. Dai, J. Wang, L. Shan, G. Niu, Q. Fan and X. Chen, Organic Semiconducting Photoacoustic Nanodroplets for Laser-Activatable Ultrasound Imaging and Combinational Cancer Therapy, *ACS Nano*, 2018, **12**(3), 2610–2622.
14 J. Zou, P. Wang, Y. Wang, G. Liu, Y. Zhang, Q. Zhang, J. Shao, W. Si, W. Huang and X. Dong, Penetration depth tunable BODIPY derivatives for pH triggered enhanced photothermal/photodynamic synergistic therapy, *Chem. Sci.*, 2018, **10**(1), 268–276.
15 A. Maleki, J. He, S. Bochani, V. Nosrati, M. A. Shahbazi and B. Guo, Multifunctional Photoactive Hydrogels for Wound Healing Acceleration, *ACS Nano*, 2021, **15**(12), 18895–18930.
16 S. Goel, C. A. Ferreira, F. Chen, P. A. Ellison, C. M. Siamof, T. E. Barnhart and W. Cai, Activatable Hybrid Nanotheranostics for Tetramodal Imaging and Synergistic Photothermal/Photodynamic Therapy, *Adv. Mater.*, 2018, **30**(6), 1704367.
17 L. Feng, M. Chen, R. Li, L. Zhou, C. Wang, P. Ye, X. Hu, J. Yang, Y. Sun, Z. Zhu, K. Fang, K. Chai, S. Shi and C. Dong, Biodegradable oxygen-producing manganese-chelated metal organic frameworks for tumor-targeted synergistic chemo/photothermal/photodynamic therapy, *Acta Biomater.*, 2022, **138**, 463–477.
18 G. Hadziioannou and P. F. Hutten, *Semiconducting polymers: Chemistry, physics and engineering*, Wiley-VCH, Weinheim, 2000.
19 Z. Yang, W. Fan, W. Tang, Z. Shen, Y. Dai, J. Song, Z. Wang, Y. Liu, L. Lin, L. Shan, Y. Liu, O. Jacobson, P. Rong, W. Wang and X. Chen, Near-Infrared Semiconducting Polymer Brush and pH/GSH-Responsive Polyoxometalate Cluster Hybrid Platform for Enhanced Tumor-Specific Phototheranostics, *Angew. Chem.*, 2018, **57**(43), 14101–14105.
20 J. Li, D. Cui, Y. Jiang, J. Huang, P. Cheng and K. Pu, Near-Infrared Photoactivatable Semiconducting Polymer Nanoblockaders for Metastasis-Inhibited Combination Cancer Therapy, *Adv. Mater.*, 2019, **31**(46), e1905091.
21 J. Zou, L. Li, J. Zhu, X. Li, Z. Yang, W. Huang and X. Chen, Singlet Oxygen ''Afterglow'' Therapy with NIR-II Fluorescent Molecules, *Adv. Mater.*, 2021, **33**(44), e2103627.
22 J. Zou, L. Li, Z. Yang and X. Chen, Phototherapy meets immunotherapy: a win–win strategy to fight against cancer, *Nanophotonics*, 2021, **10**(12), 3229–3245.
23 I. McCulloch, M. Heeney, C. Bailey, K. Genevicius, I. Macdonald, M. Shkunov, D. Sparrowe, S. Tierney, R. Wagner, W. Zhang, M. L. Chabinyc, R. J. Kline, M. D. McGehee and M. F. Toney, Liquid-crystalline semiconducting polymers with high charge-carrier mobility, *Nat. Mater.*, 2006, **5**(4), 328–333.
24 C. Cui, X. Su, Y. Guo, J. Zhu, Z. Chen, W. Qin, Y. Guo and W. Tao, Enhancing electron transfer of a semiconducting polymer for type I photodynamic and photothermal synergistic therapy, *Front. Bioeng. Biotechnol.*, 2022, **10**, 1004921.
25 C. Wu, Y. Jin, T. Schneider, D. R. Burnham, P. B. Smith and D. T. Chiu, Ultrabright and bioorthogonal labeling of cellular targets using semiconducting polymer dots and click chemistry, *Angew. Chem.*, 2010, **49**(49), 9436–9440.
26 C. Wu, Y. Jin, T. Schneider, D. R. Burnham, P. B. Smith and D. T. Chiu, Ultrabright and bioorthogonal labeling of cellular targets using semiconducting polymer dots and click chemistry, *Angew. Chem.*, 2010, **49**(49), 9436–9440.
27 F. Ye, C. Wu, Y. Jin, Y. H. Chan, X. Zhang and D. T. Chiu, Ratiometric temperature sensing with semiconducting polymer dots, *J. Am. Chem. Soc.*, 2011, **133**(21), 8146–8149.
28 G. Yu, J. Wang, J. Mcelvain and A. J. Heeger, Large-area, full-color image sensors made with semiconducting polymers, *Adv. Mater.*, 1998, **10**, 1431–1434.
29 Y. Lin and X. Zhan, Non-fullerene acceptors for organic photovoltaics: an emerging horizon, *Mater. Horiz.*, 2014, **1**(5), 470–488.
30 J. Zou, J. Zhu, Z. Yang, L. Li, W. Fan, L. He, W. Tang, L. Deng, J. Mu, Y. Ma, Y. Cheng, W. Huang, X. Dong and X. Chen, A Phototheranostic Strategy to Continuously Deliver Singlet Oxygen in the Dark and Hypoxic Tumor Microenvironment, *Angew. Chem.*, 2020, **59**(23), 8833–8838.

31 C. Fan, S. Wang, J. W. Hong, G. C. Bazan, K. W. Plaxco and A. J. Heeger, Beyond superquenching: hyper-efficient energy transfer from conjugated polymers to gold nanoparticles, *Proc. Natl. Acad. Sci. U. S. A.*, 2003, **100**(11), 6297–6301.
32 X. Feng, F. Lv, L. Liu, H. Tang, C. Xing, Q. Yang and S. Wang, Conjugated polymer nanoparticles for drug delivery and imaging, *ACS Appl. Mater. Interfaces*, 2010, **2**(8), 2429–2435.
33 Q. Miao, C. Xie, X. Zhen, Y. Lyu, H. Duan, X. Liu, J. V. Jokerst and K. Pu, Molecular afterglow imaging with bright, biodegradable polymer nanoparticles, *Nat. Biotechnol.*, 2017, **35**(11), 1102–1110.
34 Y. Jiang, J. Huang, X. Zhen, Z. Zeng, J. Li, C. Xie, Q. Miao, J. Chen, P. Chen and K. Pu, A generic approach towards afterglow luminescent nanoparticles for ultrasensitive *in vivo* imaging, *Nat. Commun.*, 2019, **10**(1), 2064.
35 C. Cui, X. Su, Y. Guo, J. Zhu, Z. Chen, W. Qin, Y. Guo and W. Tao, Enhancing electron transfer of a semiconducting polymer for type I photodynamic and photothermal synergistic therapy, *Front. Bioeng. Biotechnol.*, 2022, **10**, 1004921.
36 J. Zhu, Y. Zhang, Z. Li, X. Bao, Y. Zhou, B. Ma, Y. Xie, P. Yan, Z. Wu, Q. Zhang, J. Zou and X. Chen, Tumor-microenvironment-responsive poly-prodrug encapsulated semiconducting polymer nanosystem for phototherapy-boosted Chemotherapy, *Mater. Horiz.*, 2023, **10**, 3014–3023.